Searching Mass-Balance Analysis to Find the Composition of Martian Blueberries

R. M. Olsen[1]

[1] Two Planet Life & Two Planet Steel

Corresponding author: Rif Miles Olsen (rmo@twoplanet.life)

Key Points:

- Searching mass-balance analysis is applied to find possible standard oxide composition distributions of Martian blueberries (hematite-rich spherules).
- Two previously unknown groups of possible blueberry composition distributions are found that have zero or low SiO_2 content.
- Allowable compositions need to be consistent with the non-detection of silicates in blueberries by *Opportunity*'s Mini-TES instrument.
- Searching mass-balance analysis searches over spaces of filtering basaltic and dusty soil distributions.

Abstract

Searching mass-balance analysis is applied to find possible standard oxide composition distributions of Martian blueberries (hematite-rich spherules). This found three groups of complete solution sets to the mass-balance equations consistent with the non-detection of silicates in blueberries (by NASA's rover *Opportunity*). Two of these groups were previously unknown. One of the groups has blueberry (standard oxide) distributions nearly identical to one found in 2006, with 99.7 wt% FeO/Fe_2O_3, 0.3 wt% Ni, and zero content for other oxides. Two of ten investigations found a very small group with composition intermediate to the others. The largest group of 152,501 complete solution sets have blueberry distributions with average iron oxide content of 91.2 (± 2.9) wt% and Ni content of 0.30 (± 0.06) wt%. The main distinguishing feature between the groups is that the blueberry distributions of the largest group have five oxides/elements (MgO, P_2O_5, Na_2O, SO_3, and Cl) with a collective, summed weight percentage that averages 6.7 (± 2.2) wt%. This result is robust to changes in an SiO_2 cut-off that determines inclusion/exclusion in the larger group. Searches over spaces of filtering distributions of basaltic and dusty soils were a methodological advance. The results significantly narrow the possible range of iron oxide weight percentage in blueberries from the conclusions of previous major papers concerned with blueberry composition. The allowed levels of iron oxide are so high, and top, loose blueberries are so plentiful, that blueberries are an attractive source material to start the construction of steel infrastructure for science on Mars.

Plain Language Summary

The paper analyses data from NASA's *Opportunity* rover to find the composition of Martian blueberries. These are roughly spherical, small (1–8 mm diameters), and look blue when seen against the rusty reds of Mars. *Opportunity*'s scientists realized Martian blueberries contain a lot of an iron oxide called grey hematite within days of discovering them in January 2004. However, the resolution of how much hematite and what else blueberries contain remained low, even after years of effort from the *Opportunity* team. There are vast numbers of loose blueberries lying on top of soils covering a flat plain larger than Lake Superior. A small fraction could be harvested (picked from the soil) and then converted into steel infrastructure such as science laboratories, solar concentrators for electricity generation, landing/take-off pads for space-ships, water liberation equipment, storage tanks (for breathable air, water, rocket propellant, and more), and even radio telescopes. The analysis found a previously unknown group of likely blueberry composition distributions (with around 90% hematite content) that is consistent with an important non-detection of silicate minerals by *Opportunity*'s instruments – this is good for converting blueberries into science infrastructure on Mars.

1 Introduction

NASA chose to land its Mars Exploration Rover (MER) *Opportunity* on the Meridiani Planum (Christensen & Ruff, 2004; Christensen et al. 2005). This is a plain with an area larger than Lake Superior that straddles the equator of Mars (Edgett, 1997). In the late 1990s and early 2000s, a thermal emission spectrometer (TES) orbiting above Mars (in the *Mars Global Surveyor*) found signals of surface crystalline, grey hematite (Fe_2O_3) across the plain (Christensen & Ruff, 2004; Christensen et al. 2005). Edgett (1997) and this TES hematite data provided evidence for abundant flowing water in the plain's far past (Edgett & Parker, 1997; Christensen et al., 2000),

since hematite only forms in the presence of water. NASA considered the plain an excellent place to search for signs of life (Christensen et al. 2005).

Opportunity made a bouncing landing (Braun & Manning, 2007) into Eagle Crater on the plain in January 2004. The very first image taken by the scientific PanCam (Bell et al., 2003) had poor exposure, but it showed an expanse of soil spread from the bottom of the 22 meter diameter crater to the crater's rim and, near the limit of the camera's resolution, the image showed the soil covered with thousands of small spherules. In the coming sols (Martian days), *Opportunity*'s team found that the small spherules are rich in grey hematite (Klingelhöfer et al., 2004; *see also* Bell et al., 2004; Christensen et al., 2004; Rieder et al., 2004), and, when seen against rusty-red soils, that they look blue. The team quickly called them blueberries.

Opportunity's PanCam directly imaged huge numbers of blueberries during the rover's years-long traverse from Eagle Crater to Endeavour Crater (Calvin et. al, 2009; *see also* Fenton et al., 2015; Arvidsen et al., 2006; Soderblom et al., 2004; Squyres et al., 2004). It was soon realized that loose blueberries on top of soil were probably responsible for the regional-scale (>150,000 km^2) surface hematite detection made earlier by the orbiting TES (Squyres et al., 2004).

A recent paper introduced an idea to harvest blueberries with robotic harvesters (Olsen, 2021a). The point of such harvesting is to convert a small fraction of the blueberries into sheet steel and steel powder, then robotically construct steel infrastructure to support science on and from the plain (Olsen, 2021a). One subject omitted from that paper is the detailed composition of hematite-rich blueberries. This subject is, of course, of practical importance to iron- and steel-making on the plain and is still under-resolved, even after years of efforts by *Opportunity*'s team of scientists. The current paper takes steps toward resolving the composition of blueberries to an extent necessary for carrying out steel-making in support of science on the Meridiani Planum.

This paper is a data analysis paper. The data analyzed comes from public domain databases; particularly important here is *Opportunity*'s alpha-particle x-ray spectrometer (APXS) oxide abundance (weight percentage) database (Mars Exploration Rover APXS Team, 2016). The paper will:

1. Review the instruments that measured blueberries, in particular, what the instruments actually measured. Review the literature on blueberry composition, including the literature on mass-balance analysis applied to blueberry data, and, also, on experiments that add important constraints to blueberry mass-balance analysis (section 2).
2. Describe the choice of input APXS data used here (*i.e.,* from among the entire APXS database) (section 3).
3. Describe the demixing problem of inferring blueberry compositions from mixed signals from mixed materials. Introduce spaces of filtering distributions of basaltic soil and dusty soil compositions. (section 4).
4. Describe the searching mass-balance analysis procedure (section 5).
5. Present results from the searches (section 6).
6. Discuss these results, state conclusions, and outline milestones for future blueberry composition studies (section 7).

2 Background

2.1 *Opportunity*'s Instruments:

Opportunity's Athena suite of scientific instruments (Squyres et al, 2003) included several that could collect data useful for determining the composition of blueberries. The most focused for composition determinations were a Mössbauer spectrometer (Klingelhöfer et al., 2003) and an APXS (Rieder, 2003). However, *Opportunity*'s Mini-TES (Christensen et al., 2003), Microscopic Imager (MI) (Herkenhoff et al., 2003), PanCam (Bell et al., 2007), and even its rock abrasion tool (Gorevan, et al., 2003) all contributed data relevant to the composition of blueberries.

The Mössbauer spectrometer collected data on the abundances of minerals containing iron, while the APXS instrument collected data on the abundances of 16 elements commonly found in rocks, soils, and dust. Although, APXS abundances are reported as standard oxide abundances rather than as elemental abundances (Rieder et al., 2003). Important papers reporting the collection of APXS and Mössbauer data include Squyres et al. (2004), Reider et al. (2004), Klingelhöfer et al. (2004), Morris et al. (2006), and Gellert et al. in (2006). Klingelhöfer et al. (2004) reported the well-known, early "berry bowl" Mössbauer spectrometer experiment that showed hematite dominates the iron-containing minerals in blueberries.

Opportunity's MI made many images of interior sections of blueberries (both freshly cut by the rock abrasion tool and in blueberry fragments). These sections consistently showed that blueberries have homogeneous interiors without features resolvable at the MI's 30-32 per pixel resolution (Squyres et al., 2004). This homogeneity makes it possible to extrapolate APXS and Mössbauer surface results to whole blueberries.

2.2 Data Collection Techniques, Mixed Signals

The Mössbauer spectrometer and the APXS were used with similar surface data collection techniques; that is, each instrument was positioned at a fixed distance from the surface of target materials to be measured (using a robot arm and surface contact plates), then the instruments emitted radiation onto the targets, and simultaneously sensed, measured, and recorded back-radiation.

The input data to a blueberry composition analysis (from either the Mössbauer spectrometer or the APXS) are *mixed signal data from multiple materials*. There are two points to make about how and why this is so. The first is that the fields of view of both instruments were large relative to the view area of a single blueberry, even a large one (Squyres et al., 2004; *see also* Klingelhöfer et al., 2003; Reider et al., 2003). So the composition signals from blueberries were mixed with those from laterally adjacent materials (Squyres et al., 2004). The second is that all surface materials on Mars are covered by layers of dust and the thicknesses of these layers are not negligible relative to the sampling depth of the Mössbauer spectrometer and the APXS (Morris et al, 2006; *see also* Jolliff, 2005). Thus, since *Opportunity* had no means to clean the dust off collections of loose blueberries, blueberry composition signals were also mixed with dust signals (Jolliff, 2005; Jolliff et al., 2007a; Jolliff et al., 2007b; Morris et al, 2006). Further, although the sampling depth of the Mössbauer spectrometer was shallow (0.2–3 mm [30, 19]), that of the APXS was shallower (0.02 mm [25]); Morris et. al. (2006) emphasized that the two instruments sensed significantly different material mixtures, even when placed over the same sample targets.

152 2.3 Experimental Results to Add Constraints to Mass-Balance Analysis
153 The demixing reported here uses mass-balance analysis applied to APXS data (and
154 (possibly in a sequel paper to Mössbauer spectrometer data). A necessary, integral part of any
155 mass-balance analysis are computations using constraint equations, constraint bounds, and
156 constraint sums. However, such mathematical constraints are never enough with mixed material
157 signals. Additional constraints are needed. These should be based either on experimental data, or,
158 at least, some plausible argument or theory. The present balance analysis uses extra experimental
159 data, which is now introduced.
160 *Opportunity*'s Mini-TES instrument and PanCam made measurements that indicate that
161 blueberries have high levels of crystalline hematite (Bell et al., 2004; Calvin et al., 2009;
162 Christensen et al., 2004). These results are not specific enough to draw highly resolved hematite
163 fractions in blueberries, however, any APXS data demixing should find high levels of iron oxide
164 content, and any Mössbauer data demixing should find high levels of hematite.
165 *Opportunity*'s Mini-TES instrument made even more important measurements for
166 strongly restricting possible compositions of blueberries; that is, this Mini-TES could *not* detect
167 silicate minerals above its detection threshold (Calvin et al., 2009). This null result imposes an
168 upper bound on the size of the SiO_2 fraction in APXS blueberry compositions.
169 Features of basalt and spherule analog composition (in Mars meteorites landed on Earth,
170 in native Earth basalts, and Mars analogs on Hawaii) (Morris et al., 2005; *see also* Dunham et al.,
171 2019; Pang et al., 2008; Tirsch et al., 2012) are reflected in the initial mass-balance results
172 reported below. These features were used in an indirect way in the searching mass-balance
173 analysis to infer the composition of blueberries. In particular, these searches were influenced by
174 Morris et al. (2006) (more in section 5).
175
176 2.4 Early Blueberry Composition Mass-Balance Analysis
177 Jolliff (2005) was the first to perform mass-balance analysis on material mixtures to
178 determine the composition of blueberries. He was followed by Morris et al. (2006), and Jolliff et
179 al. (2007b) made another short analysis.
180 Morris et al. (2006) only considered cases in which the blueberry-containing mixed-
181 materials contained just three component materials: blueberry material, basaltic soil, and dust.
182 This is sensible, as (A) *Opportunity*'s sample targeting focused on these cases, and (B)
183 considering blueberry mixtures containing four or more component materials (such as
184 blueberries, basaltic soil, dust, and sediment rock) complicates the analysis. In Jolliff's first,
185 short 2005 discussion of blueberry demixing, he considered mass-balance analysis on a three-
186 component mixture of blueberry material, basaltic soil, and rock, he also mentioned this did not
187 account for the effect of dust. The principal mass-balance equation for analyzing mixtures of
188 blueberry material, basaltic soil, and dust is as follows:
189
190 Equation (1): $$p^{M}{}_{k} = m^{bb}\, p^{bb}{}_{k} + m^{bS}\, p^{bS}{}_{k} + m^{D}\, p^{D}{}_{k}, \qquad \text{for all } k,$$
191
192 In the above equation $p^{M}{}_{k}$, $p^{bb}{}_{k}$, $p^{bS}{}_{k}$, and $p^{D}{}_{k}$ are weight percentages (or, alternatively, weight or
193 mass fractions) for the material mixture (M), the blueberry material (bb) (either whole blueberries
194 and/or blueberry fragments), the basaltic soil (bS), and the dust (D); while m^{bb}, m^{bS}, and m^{D} are
195 mixing fractions (which sum to 1) for the blueberry material, the basaltic soil, and the dust.
196 Further, in Equation (1), the subscript index k that appears in the weight percentages (such as
197 $p^{bb}{}_{k}$) is an index indicating either a chemical species (for example, SiO_2) in APXS data, or a iron-

containing mineral (for example, olivine) in Mössbauer spectrometer data. Equation (1) is, in fact, a set of equations, one each for each possible value of the *k* index, and these equations need to be solved simultaneously.

Morris et al. (2006) tested an extreme APXS composition for blueberries with 99.7 wt% FeO/Fe_2O_3, 0.3 wt% Ni, and 0 wt% for all the other 14 oxide/elements. That is, this assumed blueberry composition, plus guessed mixing fractions, and an average mixed-material composition were plugged into the set of 16 equations of Equation (1) to compute a composition of mixed basaltic and dusty soils. They then presented a comparison of this computed mixed soil distribution to an average mixture of basaltic and dusty soils. These two mixed soil distributions looked very similar to the eye. Morris et al. (2006) had succeeded in showing that mass-balance analysis of blueberry/basaltic soil/dusty soil mixtures allowed blueberry compositions with close to 100% hematite content. However, in the conclusions of Morris et al. (2006), the iron oxide content of blueberries was only weakly restricted to a broad range: 24–100 wt %. This is not unreasonable in that mass-balance analysis can be applied to blueberry/basaltic soil/dusty soil mixtures using other mixing fractions and small changes to the compositions of filtering distributions to come up with blueberry compositions with very low iron oxide content. However, this conclusion of Morris et al. (2006) is far from satisfying. It is important to further constrain mass-balance analysis of blueberry/basaltic soil/dusty soil mixtures. This paper shows that, with the additional silicate mineral constraint of Calvin et al. (2009), the iron oxide content in blueberries can be restricted to a much narrower range than the 24–100 wt % of Morris et al. (2006).

Jolliff et al.'s (2007b) conference abstract on blueberry composition applied Equation (1) using two pairs of sets (of assumed) mixing fractions. (In two pairs the dusty soil mixing fraction was set to 0, while in the other pair the basaltic soil mixing fraction was set to 0.) And, in all four of these mixing fraction cases, it was assumed, with seeming reasonableness, that all the (mixed material, basaltic soil, and dusty soil) weight percentages were averages across the relevant APXS data. In the four cases, Jolliff et al. (2007b) computed blueberry weight percentages by solving Equation (1) after inputting their values on the mixing fractions and averaged weight percentages in their distributions for the mixed materials, basaltic soil, and dusty soil. Given the average distributions used, the values of the mixing fractions had been chosen so that small changes to the non-zero mixing fractions produced blueberry compositions that flipped from being allowable to dis-allowable (that is, their computations produced some blueberry weight percentages that were negative – negative weight percentages are not physically possible). Jolliff et al. (2007b) then stressed these results imposed upper limits of around 60 wt% on the FeO/Fe_2O_3 percentages in blueberries. Their upper limit was far below the 99.7% FeO/Fe_2O_3 weight percentages of Morris et al. (2006). Further, at their upper limit on iron oxide content, their computed SiO_2 weight percentages were close to 20 wt% and these SiO_2 weight percentages are *not* reconcilable with the Mini-TES results on the silicate content of blueberries (Christensen et al. 2004; Calvin et al., 2009).

3 Data Preparation

The APXS data analyzed in this paper comes from *Opportunity*'s oxide abundance database stored in the file apxs_oxides_mer1.Opportunity.csv (Mars Exploration Rover APXS Team, 2016).

Each record in the database file is a composition distribution measured from a sampling target by the APXS instrument. Only some of the distributions in the APXS database file are

used in demixing to determine the compositions of blueberries. The choices of which distributions to input to demixing computations were made using: (I) the documentation for the database file, (II) a distribution clustering procedure (more below), (III) visual checks of *Opportunity*'s MI images taken to document the sampling targets from which the APXS took distribution measurements, also, (IV) some comments in published papers. Additional details on how distributions were chosen is given in an appendix.

Mixed-Material Distributions (to be demixed)			**Basaltic Soil (filtering distributions)**		
Database Distribution ID	Shortened Distribution ID	Informal Database Name	Database Distribution ID	Shortened Distribution ID	Informal Database Name
B369_CS	B369	Crest_RippleCrest	B3373_CS	B3373	QueenAdelaide
B910_CS	B910	Marchena	B011_CS	B011	Tarmac
B080_CS	B080	JackRussel_SoilBesi	B249_CS	B249	Rocknest_void_soil
B420B_CS	B420B	RippleCrest_MayNoRooz	B166_CS	B166	Soil_Millstone_Dahlia
B505_CS	B505	Purgatrough_ThroughPlain	B3630_CS	B3630	MulgraveHills
B370_CS	B370	Caviar_undisturbedSoil	**Dusty (Top-Layer) Soil (filtering distributions)**		
B2224_CS	B2224	OceanWatch	Database Distribution ID	Shortened Distribution ID	Informal Database Name
B443_CS	B443	Recovery_Cure	B3836_CS	B3836	RockCreek
B1136_CS	B1136	Sevilla	B123_CS	B123	HillTop_Wilson
B416_CS	B416	Mobarek_undist_soil	B060_CS	B060	MontBlanc_LeHauches
			B3475_CS	B3475	YGB

Table 1: List of Distribution Identifiers. The numbers in these IDs refer to the sol on which the APXS measured the target samples.

The list of identifiers of APXS distributions used in demixing is given in Table 1. The shortened database IDs will be used here to identify distributions.

The distribution clustering to choose distributions proceeded by (A) computing a matrix of similarity distances between all pairs of composition distributions for the database's 36 composition distributions for undisturbed soils, followed by (B) matrix blocking. The blocked matrix is in Figure 1, with the pairwise similarity distance values converted to a monochrome (red-to-white) scale. The pairwise distances computed for this matrix were Jensen-Shannon distances. (Jensen-Shannon distances are used to compare distributions, they are the square roots of other distribution similarity measures, called symmetric relative entropies or Jensen-Shannon divergences; a readable reference is the Wikipedia page for Jensen-Shannon divergences.)

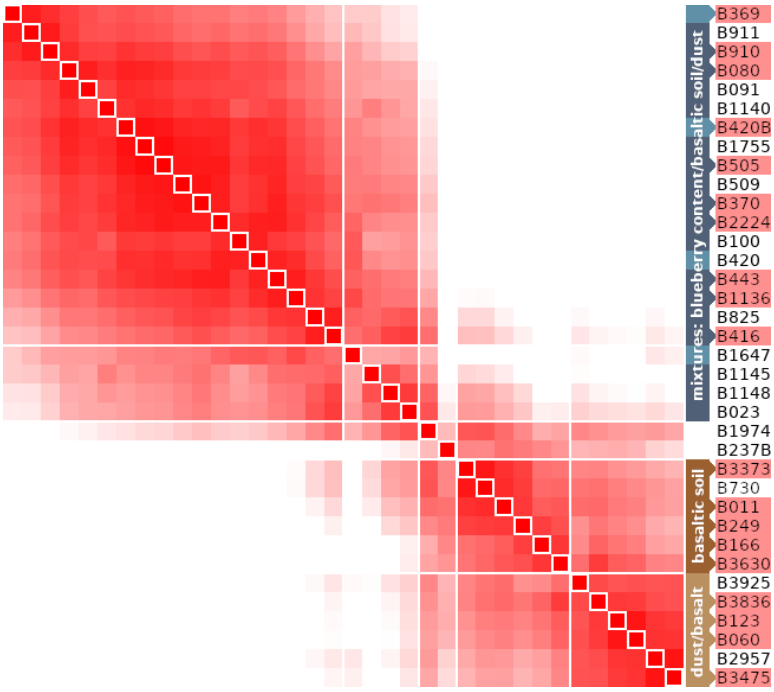

Figure 1: Blocked matrix of similarity distances between pairs of distributions.

Relevant images taken by *Opportunity*'s MI are NASA's *Opportunity* Microscopic Imager raw image archive (Mars Exploration Rover Microscopic Imager Team, 2016). Figure 2 (covering two pages) reproduces the rover's MI images from the mixed material sampling targets with distributions chosen for demixing. In addition, Figure 2(k) is an MI image of a basaltic soil that was the sampling target for APXS distribution B249, and Figure 2(l) is an MI image of the dusty (top-layer) soil that was the sampling target for distribution B3475. *Opportunity*'s MI archive did not contain images for all of the basaltic soil and dusty soil APXS sampling targets. Figure 2(k) and 2(l) are representative of those basaltic and dusty soil images in the archive.

The weight percentages of the chosen mixed material distributions are reproduced (from the APXS database) in Table 2 in the order given in the largest matrix block in Figure 1. This order makes visible rising and falling weight percentage trends across the table rows, for some of the abundant oxides such as CaO, Al_2O_3, SiO_2, and FeO, and also for some of the other oxides/elements that will be important for the demixing, including TiO_2, K_2O, and Ni, as well as the lack of rising/falling trends for some oxide/elements including MgO, P_2O_5, Na_2O, SO_3, and Cl, again these relatively constant weight percentages fractions will be important in demixing. Computed Pearson correlation coefficients (not shown) comparing the weight percentages in Table 2 for CaO, Al_2O_3, SiO_2, TiO_2, K_2O, FeO, and Ni show strong positive correlations between the weight percentages of all of CaO, Al_2O_3, SiO_2, TiO_2, and K_2O, strong anti-correlations between the weight percentages of all of these oxides and those of both FeO and Ni, and a strong positive correlation between the weight percentages of FeO and Ni.

Five of the basaltic soil distributions and four of the dusty top-layer distributions were chosen (see Figure 1 and Table 1) as filtering distributions in the demixing computations. The weight percentages for these filtering distributions are reproduced in Table 3 from the APXS oxide abundance database, with the ordering of distributions following that of the second-largest matrix block matrix Figure 1.

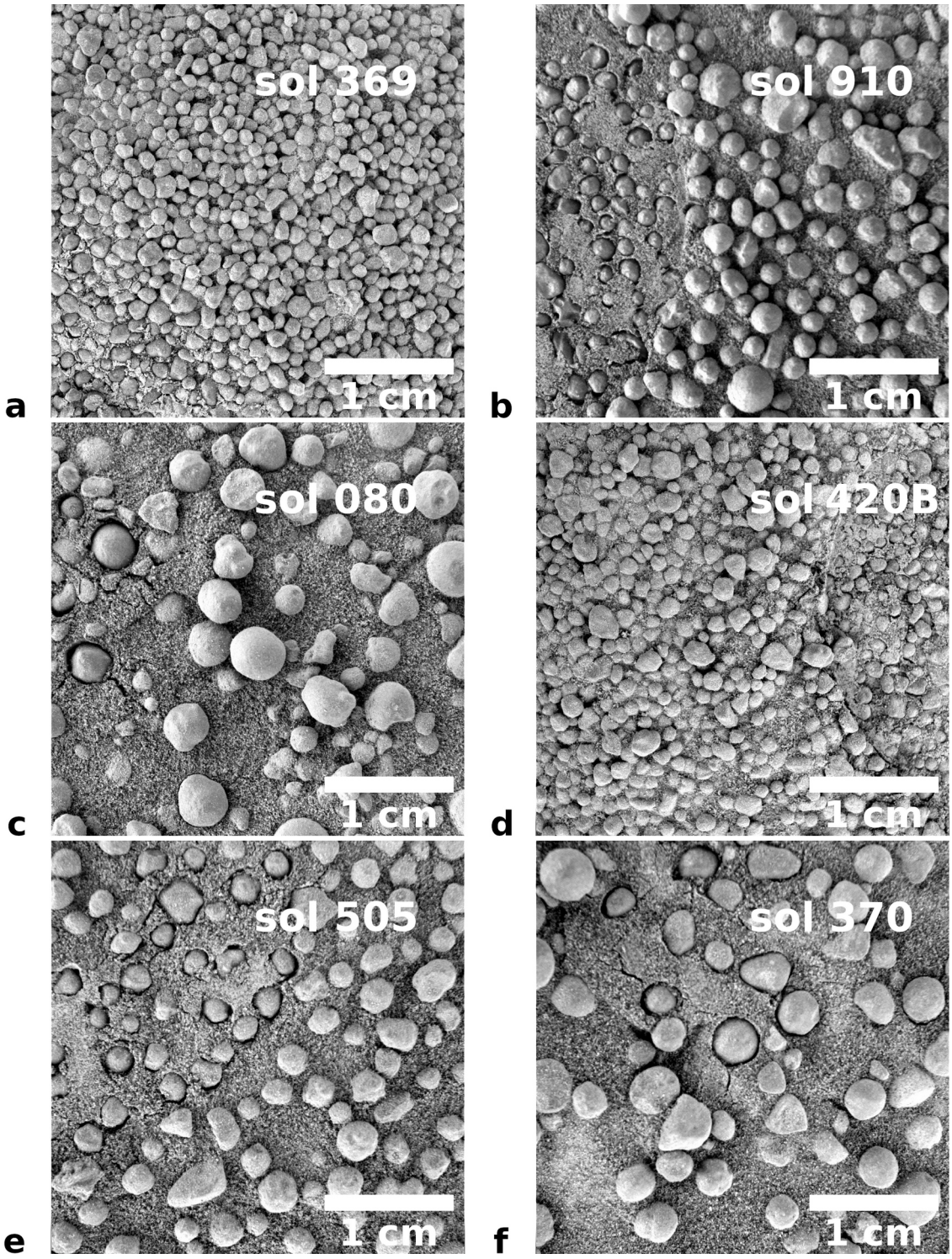

Figure 2 (first page): Sampling targets. These are discussed in the text. The order given follows the distribution order in the largest block in the matrix given in Figure 1. The sol on which each target was photographed is overlaid. NASA's *Opportunity* archive IDs for these images are (in order): 1M160940202EFF42D9P2956M2M1.JPG, 1M208971634EFF748BP2957M2M1.JPG, 1M135292637EFF10CGP2956M2M1.JPG, 1M165468362EFF5208P2956M2M1.JPG, 1M173018037EFF55VWP2956M2M1.JPG, and 1M161026325EFF42D9P2957M2M1.JPG

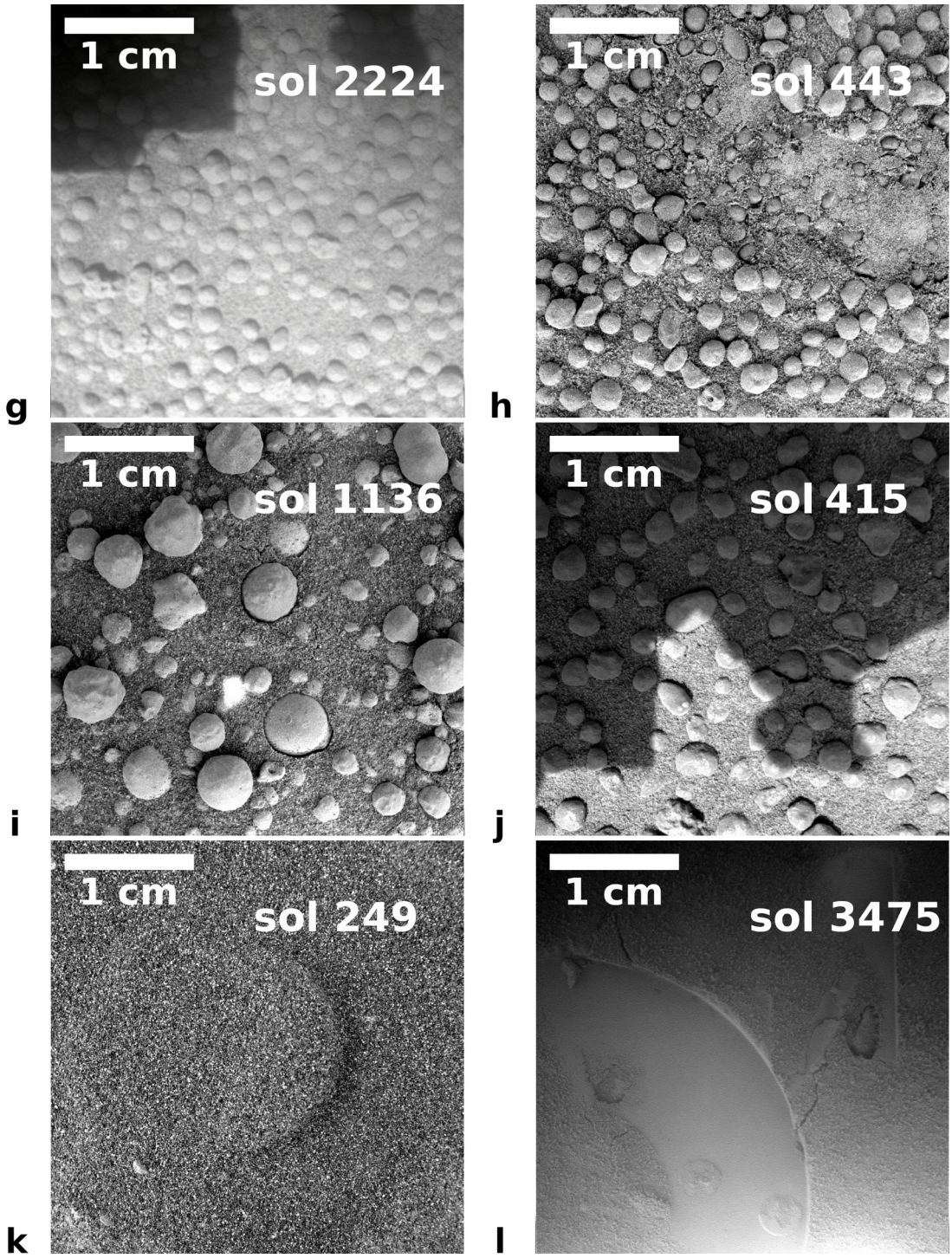

Figure 2 (second page): Sampling targets. The order given follows the order in the matrix of Figure 1. The sol on which each target was photographed is overlaid. *NOTE, the image given for distribution B416 was actually taken on sol 415 – the archive had no image that definitely shows the sampling target for distribution B416.* NASA's *Opportunity* archive IDs for these images are (in order): 1M325620114EFFAG00P2939M2M1.JPG, 1M167510573EFF55B0P2956M2M1.JPG, 1M229031407EFF81D2P2936M2M1.JPG, 1M165026294EFF5200P2956M2M1.JPG, 1M150287403EFF3620P2976M2M1.JPG, and 1M436679762EFFC9EIP2935M2M1.JPG.

	B369	B910	B080	B420B	B505	B370	B2224	B443	B1136	B416
CaO	4.88	5.04	5.10	5.27	5.39	5.67	5.55	5.69	5.96	6.17
TiO_2	0.67	0.70	0.68	0.78	0.75	0.78	0.78	0.79	0.82	0.85
K_2O	0.33	0.36	0.37	0.36	0.39	0.40	0.39	0.43	0.42	0.42
MnO	0.29	0.27	0.27	0.29	0.28	0.29	0.26	0.32	0.29	0.33
Cr_2O_3	0.27	0.30	0.30	0.27	0.32	0.32	0.32	0.32	0.31	0.33
Al_2O_3	7.36	7.39	7.66	7.76	7.80	7.83	7.78	7.78	7.79	8.19
SiO_2	37.40	37.90	38.60	39.00	39.30	39.80	39.40	40.00	40.00	41.50
MgO	6.39	6.32	6.81	6.61	6.54	6.61	6.40	6.43	6.62	6.75
P_2O_5	0.87	0.82	0.77	0.84	0.82	0.82	0.83	0.83	0.85	0.86
Na_2O	2.13	2.16	2.21	2.19	2.15	2.17	2.27	2.01	1.96	2.21
SO_3	4.64	5.28	4.90	5.15	5.24	5.05	5.54	5.54	5.89	5.21
Cl	0.71	0.73	0.68	0.70	0.65	0.68	0.72	0.72	0.75	0.67
Br	0.0101	0.0084	0.0035	0.0096	0.0048	0.0047	0.0055	0.0048	0.0083	0.0039
Zn	0.0357	0.0377	0.0304	0.0348	0.0331	0.0300	0.0332	0.0354	0.0351	0.0282
Ni	0.1292	0.1082	0.0882	0.0965	0.0743	0.0750	0.0716	0.0729	0.0660	0.0608
FeO	33.80	32.50	31.50	30.60	30.20	29.40	29.60	29.00	28.20	26.30
Total	99.9150	99.9243	99.9721	99.9609	99.9422	99.9297	99.9503	99.9731	99.9694	99.8829

Table 2 : Weight percentages of 10 distributions measured from mixed-material sample targets.

	Basaltic Soil						Dusty (Top Layer) Soil			
	B3373	B011	B249	B166	B3630		B3836	B123	B060	B3475
CaO	7.41	7.31	7.30	7.32	7.52		7.18	6.73	6.59	6.73
TiO_2	0.95	1.04	0.91	0.85	1.12		1.09	0.97	1.02	1.03
K_2O	0.45	0.47	0.48	0.55	0.55		0.49	0.51	0.48	0.52
MnO	0.47	0.37	0.40	0.39	0.34		0.34	0.37	0.34	0.36
Cr_2O_3	0.48	0.45	0.45	0.34	0.32		0.27	0.36	0.33	0.31
Al_2O_3	8.92	9.26	9.59	10.04	9.67		9.51	9.21	9.22	8.79
SiO_2	45.96	46.30	46.70	47.70	46.73		45.56	45.30	45.30	44.41
MgO	7.29	7.58	7.65	7.14	7.19		7.06	7.61	7.63	7.16
P_2O_5	0.81	0.83	0.85	0.81	0.97		1.06	0.87	0.94	1.01
Na_2O	2.10	1.83	2.39	2.40	2.30		2.21	2.38	2.24	2.25
SO_3	4.65	4.99	4.62	5.19	5.61		6.53	7.12	7.34	8.07
Cl	0.58	0.63	0.59	0.64	0.78		0.88	0.84	0.79	0.93
Br	0.0023	0.0032	0.0024	0.0025	0.0093		0.0125	0.0035	0.0026	0.0044
Zn	0.0262	0.0241	0.0184	0.0226	0.0226		0.0257	0.0376	0.0404	0.0488
Ni	0.0338	0.0423	0.0344	0.0339	0.0285		0.0282	0.0503	0.0470	0.0482
FeO	19.83	18.80	18.00	16.60	16.79		17.76	17.60	17.60	18.33
Total	99.9673	99.9296	99.9852	100.0290	99.9504		100.0064	99.9614	99.9100	100.0014

Table 3: Weight percentages of the distributions measured from basaltic soil and dusty top-layer sample targets.

4 Searching Mass-balance Analysis and the Spaces of Basaltic & Dusty Soil Filtering Distributions

There is variety between the ten mixed-material sampling targets shown in Figure 2 and between the distributions given in Tables 2 and 3.

Mass-balance analysis of mixed-material signals to find the composition of one material (*e.g.*, blueberries) in the mixture is essentially a filtering procedure to subtract (filter) the potential signals from the mixture's other materials (*e.g.*, basaltic soil and dusty soil) from the mixed signals (*e.g.*, the data in Table 2) to uncover the composition signal from the material of interest (blueberries). In the cases investigated, *i.e.*, *Opportunity*'s mixed-material sampling targets, there is no accurate and precise knowledge of the composition of the basaltic and dusty soils at each sampling site. However, there is information (in Table 3) on the compositions of basaltic and dusty soils at various other sampling locations. Using averaged basaltic and dusty soil distributions as filters on the mixed signals failed to find blueberry compositions consistent with the non-detection of silicate minerals by the Mini-TES instrument. Given this, it makes sense to search thoroughly with *different*, acceptable pairs of filtering distributions (where one is a possible basaltic soil distribution, and the other is a possible dusty soil distribution); and, with each different filtering pair, to subtract signals to find an example blueberry composition. And repeat this to find many blueberry composition examples that are consistent with the non-detection of silicate minerals in blueberries. The above is an outline of the searching mass-balance analysis done to produce the results reported here. The main search is over pairs of distributions. Section 5 gives more detail. The next thing to do is to describe the spaces of basaltic and dusty soil distributions.

4.1 Variety and the Spaces of the Filtering (Basaltic Soil and Dust) Distributions

Each basaltic soil and dust distribution in Table 3 was measured by *Opportunity*'s APXS at specific sampling locations along the rover's traverse across the plain from Eagle Crater then to and around Endeavour Crater. The physical distances between some pairs of these sampling locations were over 20 km (for example, the sampling locations for the two basaltic distributions B3373 and B011). The five basaltic soil distributions given in Table 3 (*i.e.*, B3373, B011, B249, B166, and B3630) should collectively represent practical guides as to how much variety in basaltic soil distributions could be measured across the parts of the plain traversed by *Opportunity*. Similarly, the four dusty soil distributions (*i.e.*, B3836, B123, B060, and B3475) should collectively represent practical guides to the variety of dusty soil distributions.

This paper will use these two collections to define spaces of basaltic soil and dusty soil distributions. The point of these spaces of distributions is to define acceptable basaltic soil and dusty soil distributions to use as filters in demixing calculations with the mass-balance equations (Equation (1)). So, for any given distribution used as a filtering basaltic soil distribution, that distribution must be in the space of basaltic soil distributions. Of course, the extent of the space of acceptable basaltic soil distributions should be based on the experimentally measured basaltic soil distributions.

The space of dusty soil distributions and the space of basaltic soil distributions are both defined as a central core space plus an extension layer around the core. The central core space of dusty soil distributions is, for our practical purposes, all those distributions that can be made "in-between" the four experimentally measured dusty soil distributions (*i.e.*, B3836, B123, B060, and B3475) as linear combinations of these four experimental distributions (with non-negative mixing fractions that sum to 1). Similarly, the central core space of basaltic soil distributions is

all those distributions that can be made "in-between" the five experimentally measured basaltic soil distributions (*i.e.*, B3373, B011, B249, B166, and B3630) as linear combinations these five experimental distributions (with non-negative mixing fractions that sum to 1).

A helpful analogy for these core spaces is a room. The "room" for the dust core space is a tetrahedron with the four experimental distributions (B3836, B123, B060, and B3475) forming the room's "corners," that is, the tetrahedron's vertices. Any "in-between" distribution is a point inside the room. The distances between any interior point to one of the room's corners tend to be shorter than those from one corner to another. With Jensen-Shannon distance measurement, this is also a feature of the interior dusty soil distributions and the "corner" experimental distributions (B3836, B123, B060, and B3475). Similar comments hold for the basaltic soil core space defined by the five experimental distributions (B3373, B011, B249, B166, and B3630), except now the "room's" shape is a hexahedron with five vertices or corners. Note, the two core "rooms" contain the average basaltic soil and dusty soil distributions, these average distributions are at the rooms' centers.

The practical point about having an extension layer around the cores is that the APXS distribution data is incomplete. *Opportunity*'s APXS could have sampled other basaltic soil or dusty soil targets and made distribution measurements that fall outside the core spaces. In fact, *Opportunity*'s APXS made measurements that *did* exactly this: The dusty soil distribution B3925 (shown in the blocked distance matrix in Figure 1) is outside the core space for dusty soil distributions. By definition, a distribution is considered to be inside the extension layer of the basaltic soil space when (a) it is not in the basaltic soil core space, and (b) the distance between this distribution and any one of the core space distributions is less than or equal to a maximum allowed layer thickness, denoted L^T, where this distance is measured either as the Jensen-Shannon distance or as the norm of the scalar product between the two distributions. The definition for the dusty soil case is similar just replace "basaltic soil" with "dusty soil" in the last sentence. So, now there is a question of what is a suitable value for L^T. It is good to use *Opportunity*'s actual data, so, for now, L^T is set equal to the Jensen-Shannon distance between the B3925 distribution (outside the dusty soil core) and the measured core dusty soil B3836 distribution. (Note B3925 is closer to B3836 than the other measured dusty soil distributions, B123, B060, and B3475.) However, further analysis of the data might provide reasons to change this initial value for L^T. With this layer thickness value set $L^T = 0.065$, the B3925 distribution is on the boundary of the allowed space of dusty soil distributions.

5 Searching Mass-Balance Computations

In the searches, for each of the ten mixed-material distributions listed in Table 2, we want to demix the mixed-material distributions to find blueberry composition distributions.

Ten searching investigations were carried out. Each of these ten investigations was for one of the ten mixed-material distributions listed in Table 2. Each single investigation consisted of 1,336,608 (1,336,608 = 13×126×816) attempts to find a complete solution set to the collection of 16 of mass-balance equations (for all of the 16 oxide indices) given by Equation (1). A complete solution set consists of (A) a set of three mixing fractions (*i.e.*, m^{bb}, m^{bS}, and m^{D} in Equation (1)), and (B) three demixed composition distributions (one each for blueberries, basaltic soil, and dusty soil) for the 16 APXS oxide/elements. To be a complete solution set, for each of the 16 oxide/element cases indexed with *k*, the three weight percentages ($p^{bb}{}_k$, $p^{bS}{}_k$, and $p^{D}{}_k$) from the three composition distributions and their corresponding mixing fractions (m^{bb}, m^{bS},

and m^D) are plugged into the right-hand-side of Equation (1) and precisely compute a value of the weight percentage $p^M{}_k$ (left-hand-side of Equation (1)) and this computed $p^M{}_k$ has to be equal the actual $p^M{}_k$ from the mixed-material distribution under investigation. (Emphasizing, equality between the computed right-hand-side and the actual $p^M{}_k$ has to hold for all k for any complete solution set to be valid). The goal of these searching investigations is to find many complete solution sets where the weight percentage value of SiO_2 in the blueberry distribution, $p^{bb}{}_{SiO2}$, is low and consistent with the non-detection of silicates in blueberries (by *Opportunity*'s Mini-TES).

For each of the ten investigations, the following was done:

1. For each of 13 sets of target constraints (more below): A large number (102,816) of input pairs of basaltic soil and dusty soil distributions were each individually sent to a procedure that varied the basaltic soil distribution and computed a set of the mixing fractions (in Equation (1)) and a full set of blueberry weight percentages (collectively a blueberry composition distribution).
2. Each individual variation and computation could fail or succeed at discovering an acceptable complete solution set that solved Equation (1) (up to 64-bit computer accuracy) for the individual mixed-material distribution under demixing investigation. If any one of the 1,336,608 tests/attempts succeeded, then all information for that test/attempt was made into a complete solution set record and stored in a database file of successful example records of complete solutions sets.

The 102,816 pairs of initial basaltic soil and dusty soil distributions were all combinations of a list of 126 basaltic soil distributions and another list of 816 dusty soil distributions (102,816 = 126×816). The 126 basaltic soil distributions were part of the core space of basaltic soil distributions. Five of these were the "corner" measured distributions (in Table 3), the remaining 121 were interior distributions in the basaltic core space. Collectively (by construction), these 126 basaltic soil distributions evenly sampled the basaltic soil core space. Similar construction methods were used to make the 816 dusty soil distributions in the core of dusty soil space but with a denser sampling. More information on the construction of these distributions is given in the README.txt file accompanying the open access database of complete solution sets (found in the ten investigations reported on here) that is now in the Zenodo repository (Olsen, 2021b).

The use of 13 sets of target constraints mentioned in the above outline was motivated by Morris et al. (2006). That paper inferred a reasonable combined filtering soil distribution (a weighted combination of basaltic soil and dusty soil distributions) by inputting into Equation (1): (A) a mixed-material distribution that was made by averaging experimental measurements; and (B) a completely specified (made-up) blueberry composition distribution with the FeO/Fe_2O_3 weight percentage set to 99.7 wt%, Ni set percentage set to 0.3% and the weight percentages of the fourteen other oxides/elements set to 0%. This method used the authors' experience with geology, blueberries, and Hawaiian blueberry analogs (Morris et al., 2005) to assert that many APXS oxides were likely to be extremely small or 0%.

In an effort to both use the idea of constraining some of the oxide/element weight percentages to 0% (with is computationally helpful) and also to be more deliberate about how many and which oxide/element weight percentages to constrain to 0%, plots of the various oxide weight percentages (found in Table 2) were made against the weight percentages of FeO (also in

Table 2). The collection of these plots (not shown) suggested the following ordering of oxides most likely to have 0 wt% in blueberries (from most likely to quite possible): CaO & TiO_2, K_2O, MnO, Cr_2O_3, Al_2O_3, and SiO_2. In addition, the weight percentages for bromine (Br) are always so low, and had other features (see discussion) that the computations could easily find some basaltic soil/dusty soil pairs that could accommodate setting the Br weight percentage to 0% (even with Br's mildly positive correlation with FeO). Although Zn also has very low weight percentages (see Tables 2 and 3), these are generally higher weight percentages than those of Br, and the Zn data does not have the confusing features that Br data has, further Zn is also moderately positively correlated to FeO, so it is hard to accommodate a 0 wt% for Zn using fine variations in soil compositions. Although MgO is noticeably anti-correlated to both FeO and Ni in mixed material distributions, this anti-correlation is not so strong as those between FeO and CaO, TiO_2, K_2O, Al_2O_3, and SiO_2, while the weight percentages for MgO in mixed materials are high. This combination of abundance and only moderately strong anti-correlation generate a question as to whether there is or is not any MgO in blueberries. In addition, the weight percentages for all of P_2O_5, Na_2O, SO_3, and Cl in mixed materials are only weakly correlated or anti-correlated with those for FeO and Ni, and the weight percentages of these species in mixed material are much larger than those of Br, Zn, and Ni. So, for all of P_2O_5, Na_2O, SO_3, and Cl, there are questions as to whether or not these species appear in blueberries. Given the above, the 13 sets of constraints used in the initial search program were sequentially constructed to be more and more restrictive. The first set constrained the weight percentages of only CaO and TiO_2 to 0 wt%. Continuing with addition by one, the seventh set of constraints fixed the weight percentages to 0 wt% for these eight oxides/elements: CaO, TiO_2, K_2O, MnO, Cr_2O_3, Al_2O_3, SiO_2, and Br. The most restrictive (thirteenth) set only left FeO and Ni free and enforced 0 wt% on the other fourteen oxide/elements.

For each input mixed material distribution, the initial program has three levels of searching. The two obvious ones are the surveys over (I) the input pairs of soil distributions and (II) the list of 13 (0 wt%) constraint sets. The third level of search is through variations to the input basaltic soil distribution. These variations are computed in 12×102,816 out of the 13×102,816 tests run for each mixed material investigation. In the least restrictive constraint set, with just two 0 wt% constraints (*i.e.*, those for CaO & TiO_2), these two constraints can be satisfied by adjusting the two free parameters of the three mixing fractions (m^{bb}, m^{bS}, m^{D}). (That is, in this least restrictive case, this adjustment fixes the values of the mixing fractions.) In the other 12 cases, the list of constraints cannot be satisfied solely by adjusting the values of the mixing fractions. In these cases, the basaltic soil distributions are varied (in addition to the mixing fractions) to enforce the longer list of 0 wt% constraints. A least-squares optimization procedure (to satisfy the given set of 0 wt% constraints) controls the variations made to the basaltic soil distributions.

Limitations with this searching procedure are discussed in section 7.

6 Results

The searches found <u>*three*</u> *groups* of complete solution sets of Equation (1) that also had blueberry SiO_2 weight percentages low enough that the Mini-TES might not have detected any silicate minerals. The complete solution sets in the two smaller group are similar to the solution set of Morris et al. (2006). These groups of complete solution sets are discussed later.

Table 4 presents three examples of complete solution sets from the largest group. These solution sets are called ES1 (Example Solution 1), ES2, and ES3. All three sets are complete

Normalized B370 Distribution		ES1 (0 wt% SiO_2 solution)			ES2 (approx. 4 wt% SiO_2 solution)			ES3 (approx. 8 wt% SiO_2 solution)		
		Blue-berries	Basaltic Soil VBS_ES1	Dusty Soil	Blue-berries	Basaltic Soil VBS_ES2	Dusty Soil	Blue-berries	Basaltic Soil VBS_ES3	Dusty Soil
	Mix Fractions	0.131358	0.678260	0.190382	0.154705	0.542889	0.302406	0.169250	0.513955	0.316795
Wt%	oxide/ element	Wt%	Wt%	Wt%	Wt%	Wt%	Wt%	Wt%	Wt%	Wt%
5.673989	CaO	0.000000	6.413284	6.955030	0.000000	6.617250	6.883325	0.000000	6.887379	6.736808
0.780549	TiO_2	0.000000	0.852454	1.062930	0.000000	0.856116	1.044202	0.000000	0.888499	1.022429
0.400281	K_2O	0.000000	0.452959	0.488791	0.000000	0.459490	0.498765	0.000000	0.471738	0.498206
0.290204	MnO	0.000000	0.332031	0.341422	0.000000	0.339927	0.349404	0.000000	0.348001	0.351480
0.320225	Cr_2O_3	0.000000	0.389953	0.292755	0.000000	0.420106	0.304737	0.000000	0.424085	0.322810
7.835508	Al_2O_3	0.000000	8.922918	9.367729	0.000000	9.296128	9.221859	0.000000	9.608095	9.145919
39.827999	SiO_2	**0.000000**	45.975034	45.408478	**3.991376**	47.061342	45.175828	**7.985826**	47.054104	45.116600
6.614650	MgO	0.772625	7.565293	7.258680	2.800440	7.333427	7.275559	2.056806	7.614304	7.427917
0.820577	P_2O_5	0.432700	0.840588	1.016907	0.361378	0.852872	0.997517	0.375598	0.880521	0.961060
2.171527	Na_2O	2.056408	2.179302	2.223252	1.819080	2.228365	2.249795	1.329206	2.389674	2.267630
5.053553	SO_3	3.547765	4.825598	6.904612	1.030702	5.013861	7.182825	1.2942830	4.853964	7.385775
0.680478	Cl	0.835382	0.601903	0.853536	0.451194	0.640159	0.870160	0.508903	0.632691	0.849672
0.004703	Br	0.010929	0.002387	0.008660	0.003110	0.003789	0.007160	0.007649	0.003809	0.004581
0.030021	Zn	0.041555	0.027189	0.032151	0.034902	0.025080	0.036395	0.043389	0.019384	0.040137
0.075053	Ni	0.311549	0.040265	0.035813	0.279348	0.036221	0.040250	0.256661	0.033467	0.045494
29.420683	FeO	91.991088	20.578841	17.749252	89.228469	18.815867	17.862220	86.141678	17.890284	17.823481

Table 4: Three Example Solutions of Mass-Balance Demixing (Equation (1)) of Mixed-Material Distribution B370.

solutions sets for the B370 mixed-material distribution (one of the ten distributions listed in Table 2). These three examples were chosen from many thousands of similar complete solution sets (more below). These three examples are not better than many other complete solution sets. They are just examples of complete solution sets with low enough blueberry SiO_2 wt% to be compatible with the Mini-TES's non-detection of silicate minerals in blueberries. Although ES3 is a borderline case, since its 8 wt% for SiO_2 may be too high for a non-detection of silicate minerals by *Opportunity*'s Mini-TES instrument. (The Mini-TES mineral abundance measurements were accurate to within 5–10 wt% (Christensen et al., 2003).) The example solution sets ES2 and ES3 were computed with six oxides (CaO, TiO_2, K_2O, MnO, and Cr_2O_5, and Al_2O_3) constrained to 0 wt%. ES1 was computed with those six oxides plus SiO_2 constrained to 0 wt%. The normalized version of distribution B370 (with a total weight percent sum of exactly 100%) is in the left column of Table 4 to six decimal place accuracy. Similarly, the mixing fractions and the weight percentages of the three complete solution sets are all given to six decimal place precision (the full records store at 15 decimal place precision or more). This precision does *not* imply a high level of certainty in our knowledge of the compositions of blueberries, basaltic soil, and dust. Rather each complete solution set is just one of many

567 solutions that all solve the mass-balance equations with equally high precision. Collectively, the
568 multitude of complete solution sets generate ranges of possible compositions for blueberries,
569 basaltic soils, and dusty soils (and the mixing fractions of these). The reason such high precision
570 is used in the searches is to find actual solutions to the mass-balance equations (Equations (1)) –
571 the calculations to find these solutions are sensitive to small changes.
572 Tables 5(a) and 5(b) give some Jensen-Shannon distances. These provide some
573 information on the distances between distributions in the space of basaltic soils, and on the sizes
574 of variations between input basaltic soils (to the surveying search) and the varied basaltic soils
575 that provide (exact) complete solution sets.
576 Table 5(a) gives a matrix of Jensen-Shannon distances between the five experimentally
577 measured basaltic soil distributions in Table 3 and the three Input Basaltic Soil distributions,
578 (IBS_ES1, IBS_ES2, and IBS_ES3) to the computations that produced the example solutions
579 listed in Table 4. For solution ES1, the input distribution IBS_ES1 is one the measured
580 distributions (B3373), so IBS_ES1 is not one of the "interior" distributions, but a "corner"
581 distribution of the core. For solutions ES2 and ES3, the input distributions IBS_ES2 and
582 IBS_ES3 are both "interior" distributions. Note, the distances between the two "interior"
583 distributions and the corner (measured) distributions are mostly smaller than the distances
584 between one measured distribution and another: Table 5(a) gives examples of distances
585 consistent with the analogy between a room and the core space of basaltic soil distributions.
586

	B3373	B011	B249	B166	B3630	IBS_ES1 = B3373	IBS_ES2	IBS_ES3
B3373	0	0.043	0.056	0.099	0.102	0	0.039	0.062
B011	0.043	0	0.050	0.081	0.077	0.043	0.033	0.049
B249	0.056	0.050	0	0.056	0.071	0.056	0.032	0.015
B166	0.099	0.081	0.056	0	0.048	0.099	0.062	0.046
B3630	0.102	0.077	0.071	0.048	0	0.102	0.065	0.056

587 Table 5(a): A matrix of Jensen-Shannon Distances between basaltic soil distributions.
588
589 Table 5(b) gives Jensen-Shannon distances between the input basaltic soil distributions
590 and the final Varied Basaltic Soil distributions (VBS_ES1, VBS_ES2, and VBS_ES3) listed in
591 the basaltic soil columns of Table 4. These distances are all smaller than the layer thickness,
592 $L_T = 0.065$, defined in section 4.
593

Input Basaltic Soil distributions	Varied Basaltic Soil distributions	Jensen-Shannon Distance
IBS_ES1	VBS_ES1	0.052
IBS_ES2	VBS_ES2	0.037
IBS_ES3	VBS_ES3	0.021

594 Table 5b: Jensen-Shannon distances between input basaltic soil distributions and varied basaltic soil
595 distributions.
596
597 The four scatter plots in Figure 3 present partial information about 189,531 complete
598 solution sets where either five, six or seven of the APXS oxides were constrained to 0 wt%.
599 These scatter plots use partial information from investigations of four mixed-material
600 distributions: B369 (Crest_Ripple), BO80 (JackRussel), B370 (Caviar) and B1136 (Sevilla).
601 These four scatter plots give FeO verses SiO_2 blueberry weight percentages. The legend boxes

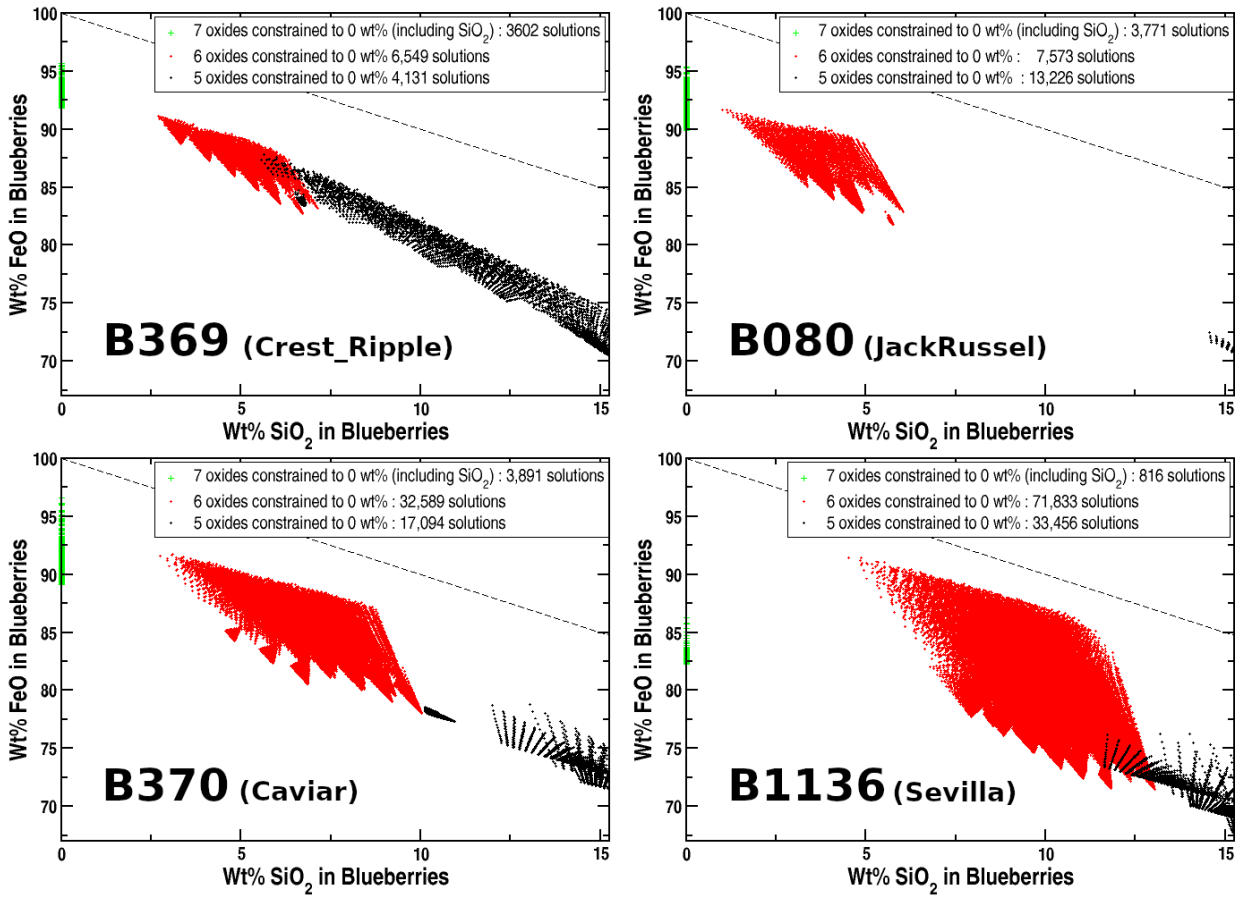

Figure 3: FeO verses SiO_2 blueberry weight percentage scatter plots.

give the number of times a complete solution set was successfully computed among 102,816 computational tests run for each each constraint set, for each mixed-material distribution investigated. Complete solutions sets where the previous seven oxides plus Br where constrained to 0 wt%, could be used to add more points to the Figure 3 scatter plots, however, these points coincided with the points from the seven oxide constraint tests. Scatter plots for the other six mixed-material distributions (*i.e.* B910, B420B, B505, B2214, B443, and B416) were similar to those shown in Figure 3.

An important point to realize about the scatter plots in Figure 3 is that they are rather misleading. They are misleading in that they are not showing +'s at all the locations where they could be placed. More complete scatter plots would be thick linear bands with the green, red and black "blobs" joined together. The gaps seen between the "blobs" in Figure 3 are artifacts of the details of the initial searching mass-balance analysis procedure. This point is returned to in the discussion.

The Figure 3 scatter plots only reach SiO_2 weight percentages of 15 wt%. However, there were other complete set solutions with higher SiO_2 weight percentages and lower FeO weight percentages. These solution sets, with higher blueberry SiO_2 content, were computed using constraint sets where either two, three, four, or (sometimes) five of the oxides were constrained to 0 wt%. These higher blueberry SiO_2 content complete solutions sets are *not* consistent with the Mini-TES instrument's non-detection of silicate minerals in blueberries.

In the scatter plots of Figure 3, the vertical distance between each point in a scatter plot and the dashed diagonal line gives the total weight percentage in blueberries for all the other oxide/element species that had more than zero weight percentage and were not FeO or SiO_2.

For the rest of the results on the largest group of complete solutions of the mass-balance equations (Equation (1)), three upper cut-offs in SiO_2 content (*i.e.*, 8 wt%, 4 wt%, and 0 wt%) are adopted for such solutions to be considered consistent with the non-detection of silicate minerals by the Mini-TES instrument. These three cut-offs give alternative operational divides for inclusion in the larger group of complete solutions. At least one cut-off value is needed and it is not very clear what an optimal cut-off value is. However, since the main new result does not change much between the three reasonable cut-off values, the new result is robust to reasonable changes in the cut-off value.

Table 6 presents averaged blueberry composition weight percentages across the largest group of complete solution sets, across the three versions of the largest group defined by the upper cut-offs in SiO_2 weight percentage. Each weight percentage row in Table 6 needs a separate discussion. The rows for SiO_2 and FeO are discussed immediately. The discussions for the other rows are given in the final section.

	8 wt% SiO_2 cutoff			4 wt% SiO_2 cutoff			0 wt% SiO_2 cutoff		
Number of solutions	311,092			152,501			83,943		
Oxide/element or group	min (wt %)	Ave. ± St.D. (wt %)	max (wt %)	min (wt %)	Ave. ± St.D. (wt %)	max (wt %)	min (wt %)	Ave. ± St.D. (wt %)	max (wt %)
SiO_2	0.000	3.553 ± 2.616	8.000	0.000	1.254 ± 1.521	4.000	0.000	0.000 ± 0.000	0.000
FeO	77.744	88.661 ± 4.065	98.332	82.252	91.170 ± 2.935	98.322	82.252	93.197 ± 2.318	98.332
Ni	0.185	0.294 ± 0.065	0.520	0.207	0.298 ± 0.062	0.531	0.237	0.322 ± 0.059	0.531
$MgO+Na_2O+P_2O_5+SO_3+Cl$	1.296	**7.421 ± 2.405**	17.365	1.296	**6.680 ± 2.222**	17.365	1.296	**6.414± 2.300**	17.365
Zn	2×10^{-5}	0.059 ± 0.015	0.101	2×10^{-5}	0.056 ± 0.014	0.101	2×10^{-5}	0.058 ± 0.015	0.101
Br	0.000	0.012 ± 0.011	0.050	0.000	0.009 ± 0.012	0.050	0.000	0.009 ± 0.016	0.050

Table 6: Blueberry composition averaged over the larger group of complete solution sets. Averages given to two significant digits in Br wt%, and to three decimal places in the others to vertically align numbers.

The averages given for SiO_2 in Table 6 are essentially those of a free parameter that is being adjusted by the value of the cutoff value. These values only make sense to the extent that the cutoff values make sense. Turning to the FeO numbers in Table 6, the changes in the weight percentage averages for FeO are strongly anti-correlated to the changes in those for SiO2, so the changes to the FeO averages are also driven by the changes in the cutoff value. However, the changes in the FeO averages are slightly larger than those in the SiO_2 averages, and, of course, the absolute values of all the FeO averages are very high (between 88 and 93 wt%), but not extremely close to 100 wt%.

Table 7 gives the number of times a complete solution set was successfully computed among 102,816 computational tests run, for different constraint set cases, for all the mixed-material distributions investigated. Some constraint set cases do not appear in Table 7. In particular, the least restrictive cases, with only 2, 3, or 4 of the oxides constrained to have zero weight percentage. For these three constraint set cases, there were many thousands of allowable

# oxides constrained to 0 wt%	Constrained Oxides	Mixed-Material Distributions									
	Always constrained: CaO & TiO_2 & K_2O & MnO	B369	B910	B080	B420B	B505	B370	B2224	B443	B1136	B416
5	Previous & Cr_2O_3	4,131	14,688	13,226	22,779	7,344	17,094	0	21,530	33,456	18,108
6	Previous & Al_2O_3	6,549	56,737	7,573	5,626	44,917	32,589	61,611	59,706	71,833	12,428
7	Previous & SiO_2	3,602	816	3,771	8,730	3,606	3,891	807	0	816	1,149
8	Previous & Br	0	0	20,749	0	10,146	10,576	4,197	207	0	10,880
9	Previous & Zn	0	0	0	0	0	0	0	0	0	211
10	Previous & MgO	0	0	0	0	0	0	0	0	0	68
11	Previous & P_2O_5	0	0	0	0	0	0	0	11	0	0
12	Everything EXCEPT FeO, Ni, Cl, & SO_3	0	0	0	0	0	0	0	457	2,989	0
13	Everything EXCEPT FeO, Ni, & Cl	0	0	0	0	0	0	0	12,927	7,444	0
14	Everything EXCEPT FeO & Ni	0 (0)	0 (776)	0 (813)	0 (3,595)	4,765 (45,463)	802 (4,004)	0 (11,724)	88 (11,540)	8 (9,656)	7,915 (17,393)

Table 7: Number of allowed solutions to Equation (1) found in sets of 102,816 searches for each of the 10 mixed-material distributions. The numbers in parentheses for the most restrictive constraint set, are the numbers of complete solution sets that precisely solved Equation (1), but for which the varied basaltic soil distribution in the solution was not part of the allowed basaltic soil distribution space.

complete solutions, however they all had weight percentages for SiO_2 that were not consistent with the Mini-TES instruments non-detection of silicate minerals. The same is true of almost all the complete solution sets with 5 of the oxides constrained to have zero weight percentage; however, a small minority (see Figure 3) of the 4,131 solutions with 5 oxides constrained for the B369 investigation had SiO_2 weight percentages between 4 wt% and 8 wt% (this small number of solutions was not used for the statistics counted for the largest group of complete solution sets).

The complete solution sets included in the largest group were all of those with 7 or 8 oxides constrained to 0 wt% (their SiO_2 levels were always 0 wt%) and all those solution sets with 6 oxides constrained to 0 wt% that also had SiO_2 levels below the cut-offs.

In nine of ten investigations zero complete solution sets were found with 9 or 10 oxides constrained to 0 wt%. The small number (211 + 68) of complete solution sets found in the B416 investigation, with 9 or 10 oxides constrained, had very similar blueberry distributions to those initially included in the largest group of solutions sets, so these are included in the largest group of solution sets (although they were not included in the statistics reported in Table 6.)

All rows of Table 7 have been discussed except those with 11, 12, 13, or 14 oxides constrained to 0 wt %. The complete solution sets associated with the last two of these rows have blueberry distributions that are very similar to expertly forced example solution of Morris et al. (2006). These solutions associated with the last two rows of Table 7 form the second main group of complete solution sets that this initial searching mass-balance investigation found. Table 8 summarizes the blueberry composition results for this second, smaller group.

# oxides constrained to 0 wt%	Mixed-Material Distributions	# solution sets*	Wt% FeO in blueberries Ave. ± St.D. (wt %)	Wt% Ni in blueberries Ave. ± St.D. (wt %)	Wt% Cl in blueberries Ave. ± St.D. (wt %)
13	B443 & B1136	20,391	99.4506 ± 0.1277	0.2597 ± 0.0020	0.2896 ± 0.1386
14	B505, B370, B443, B1136, & B416	13,578	99.7193 ± 0.0189	0.2807 ± 0.0189	0.0000 ± 0.0000

Table 8: Blueberry composition averaged over the second group of complete solution sets (most restrictive constraint set cases).

Only the B433 investigation produced any (just 11) complete solution sets for search cases with 11 oxides constrained to 0 wt%. These solution sets had blueberry composition distributions very close (results not shown) to those specified in Table 8 for the second group of solutions. These eleven solution sets should be grouped with second group of solutions.

Scatter plot Figure 4 summarizes the mixing fraction results for the most constrained computations in the B370 and B416 investigations. Figure 4 highlights a point that is especially prevalent for the results for the second group of complete solution sets. That is, many complete solutions sets were found by the searches program that precisely solved the mass-balance equations (Equation (1)); however, the variation in the input basalt soil distribution produced a varied distribution that could no longer be considered part of the space of basaltic soil distributions. Whenever a variation produced this outcome the solution could not be accepted. The numbers in parenthesis in the last row of Table 7 record how often these cases happened. The mixing fraction scatter plots in Figure 4 include points for the complete solutions that were rejected. In each mixing fraction scatter plot there is a clear separation between the accepted and rejected complete solutions.

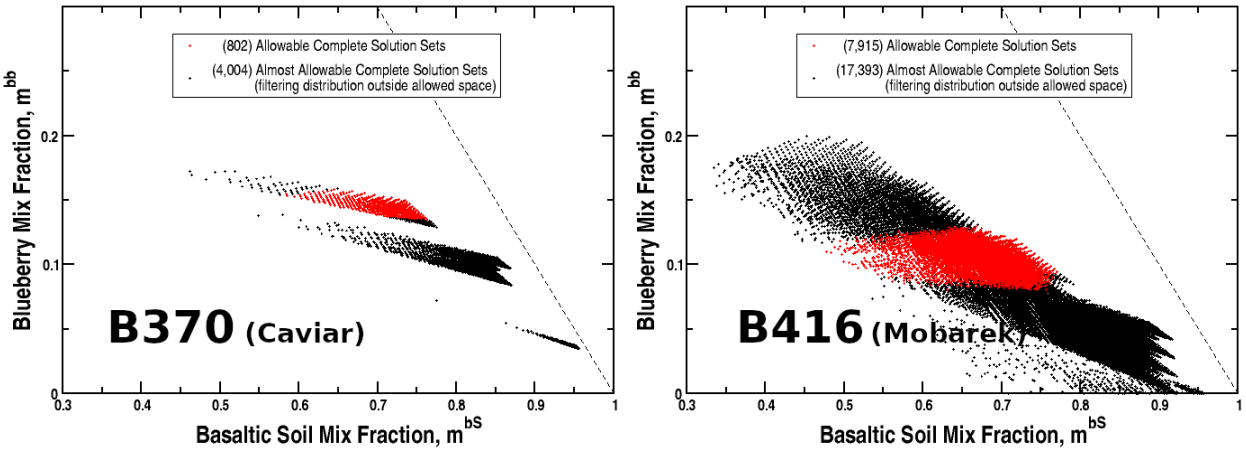

Figure 4: Mix fractions complete solutions of the smaller group.

The ten investigations found one more small group of complete solution sets, where the SiO_2 content in the set's blueberry distribution is low enough to be consistent with the non-detection of silicates in blueberries. These solutions sets were found only in the B443 and B1136 investigations with 12 oxides constrained to 0 wt %. The blueberry compositions statistics for these 3,446 (457+2,989) complete solution sets are given in Table 9.

# oxides constrained to 0 wt%	Mixed-Material Distributions	# solution sets	Wt% FeO in blueberries Ave. ± St.D. (wt %)	Wt% Ni in blueberries Ave. ± St.D. (wt %)	Wt% Cl in blueberries Ave. ± St.D. (wt %)	Wt% SO_3 in blueberries Ave. ± St.D. (wt %)
12	B443 & B1136	3,446	97.1575 ± 1.4275	0.2806 ± 0.0225	0.2674 ± 0.1123	2.2944 ± 1.355

Table 9: Blueberry composition averaged over the third (smallest) group of complete solution sets.

7 Discussion and Conclusions

The search procedure found a large group of complete solutions sets with blueberry distributions summarized by the results in Table 6. This table outlines possible blueberry distributions significantly different from those in Table 8, where the Table 8 solutions are very similar to the asserted blueberry composition of Morris et al. (2006). A third, much smaller, group of complete solution sets was found with blueberry composition distributions summarized in Table 9, that are intermediate to those in Tables 6 and 8.

The results section discussed the SiO_2 and FeO rows in Table 6. Turning to the Ni row of Table 6, it is noteworthy that the weight percentages for Ni in Tables 6, 8, and 9 are similar and close to 0.3 % (just like Morris et al. (2006)). These levels are all enhanced over the Ni levels in the distributions of Table 2. This is expected, since the Ni levels in Table 2 are, in turn, enhanced over those in the filtering distributions in Table 3. The row in Table 6 with the most uncertain, and most undetermined, results is that for Br. The Br data in Tables 3 and 4 forces this uncertainty. In all distributions given in Tables 3 and 4, the weight percentages for Br are low. However, there are large relative differences in Br levels between distributions in Table 3. In particular, distributions B3630 and B3836 have Br levels 3.5–5 times higher than distributions B249, B166, and B060. Further, although the Br levels in the mixed-material distributions in Table 2 tend to be higher than those in Table 3, the Br levels in distributions B3630 and B3836 from Table 3 are higher than most of those in Table 2. With these data features for Br, searching mass-balance calculations that allow Br to have larger than zero weight percentages will find enhanced levels of Br in blueberries because there are several basaltic and dusty soils (in Table 3) with lower Br levels than those in the mixed material distributions (in Table 2). However, if solutions are sought in which the Br level is constrained to 0 wt %, then such solutions can also be found for most of the distributions in Table 2 because the Br levels in B3630 and B3836 are so high that these can be used as filters that accommodate all the Br in the mixed materials while holding the blueberry Br content to 0 wt%. The only possible way to improve this situation is to re-process the relevant raw data to improve the accuracy and precision of the database Br weight percentages; if this re-processing found Br levels without the large relative differences now found in Table 3, then a satisfactory Br weight percentage in blueberries could be calculated.

The Zn levels in Table 2 are all enhanced over the Zn levels in the basaltic soil distributions in Table 3, while three of four of the dusty soil distributions in Table 3 have higher Zn levels than the mixed-material distributions in Table 2. This is an interesting background to the Zn levels given in the blueberry distributions in Table 6. These average blueberry Zn levels (in Table 6) are enhanced over all the distributions in both Tables 3 and 4. Given the Zn data in Tables 3 and 4, this enhancement in average blueberry Zn levels can only occur (and will occur) if the mixing fraction for the basaltic soil distribution is noticeably bigger than the mixing fraction of the dusty soil distribution in most of the complete solutions sets (in the largest solution group from which the Table 6 results are drawn). This does occur in the example solutions ES1, ES2, and ES3 given in Table 4. However, this extra mixing fraction weight given

to basaltic soil distributions relative to dusty soil distributions is not determined by solving the mass-balance equations for the Zn case; rather, this preponderance for the basaltic mixing fraction is driven by the mixed-material data in Table 2 for the oxides CaO, TiO_2, K_2O, MnO, Cr_2O_5, and Al_2O_3 (and sometimes SiO_2) and the least-squares procedure to solve the mass balance equations that ensure that the weight percentages are zero for these oxides.

There is one more row in Table 6 left to discuss, the row for the group of five species (MgO, Na_2O, P_2O_5, SO_3, and Cl). The average summed total weight percentages for these five species is remarkably high (at around 7%) and robust to changes in the cutoff value that determines which of the complete solution sets are included in the larger group. At the most conservative cutoff value of zero in the weight percentage of SiO_2 in blueberries, the average summed total weight percentages for the five species remains high at 6.4 wt%. Note, this most conservative cutoff of 0 wt% SiO_2 in blueberries corresponds to the *most extreme possible interpretation* of the Mini-TES's non-detection of silicate minerals in blueberries. That is, this 0 wt% SiO_2 in blueberries implies that blueberries contain no silicate minerals at all. So, while finding 83,943 complete solution sets in the larger group with 0 wt% SiO_2 in the blueberry distribution, it is an impressively robust result that the average total weight percent for the five species (MgO, Na_2O, P_2O_5, SO_3, and Cl) remains between 6 and 7 wt%.

In the larger group of complete solution sets, MgO, Na_2O, P_2O_5, SO_3, and Cl are in blueberries at well above trace levels. The large number of possible geochemical pathways that these five species could factor into in blueberry formation processes are significantly different to, and more flexible than, the geochemistry (and exclusion means) needed to form blueberries with the severely pure, hematite-and-nickel-only blueberry composition example asserted by Morris et al. (2006) (with 99.7 wt% FeO/Fe_2O_3, 0.3 wt% Ni and 0 wt% for all other oxide/elements). Geologically plausible blueberry formation histories that are consistent with the averaged blueberry compositions (in Table 6) of the largest group are likely much easier to posit than histories leading to the formation of blueberries with the averaged, hematite-and-nickel-only blueberry compositions (in Table 8) of the second group of complete solution sets.

The Hawaiian analogs of blueberries studied by Morris et al. (2005) have composition features that make them rather more like the blueberry compositions of the new largest group than the asserted composition of Morris et al. (2006) and the compositions of the second group. That is, the breccia HWMK745R spherule sample composition reported in Morris et al. (2005) had FeO/Fe_2O_3 content at 90.90 wt% (significantly below 99.7 wt%), SiO_2 content at 1.93 wt% (which is above-zero, but small enough to be below Mini-TES silicate detection), with a balance of around 7 wt% (although that balance was *not* mainly due to MgO, Na_2O, P_2O_5, SO_3, and Cl).

It is possible that the largest group can be divided into sub-groups based on distinct composition signatures from among the five species MgO, Na_2O, P_2O_5, SO_3, and Cl. For example, comparing blueberry composition distributions in ES1 and ES2 (Table 4), the MgO content in ES2 is much higher than in ES1, and the SO_3 and Cl content is much higher in ES1 compared to ES2. ES2, with close to 4 wt% SiO_2, is consistent with some olivine content in blueberries, ES1 is not, but ES1 is consistent with sulfur mineral content in blueberries.

The paper investigated ten different mixed-material distributions. It has not reported on the differences between the complete solution sets found in the ten investigations. This is partly due to a desire to avoid overloading the paper with subject matter, and also, in part, due to the lack of completeness of the initial results (more below). However, here are brief impressions on blueberry variability: Blueberry compositions across widely spaced sampling locations appear very similar, but there are small variations.

The main conclusions of the paper are: (1) the spaces of basaltic and dusty soil distributions enabled searching mass-balance analysis to be carried out; (2) that the searching mass-balance analysis found one large and one small new groups of complete solution sets (of the mass-balance equations) that are consistent with the non-detection of silicate minerals; (3) that the averaged blueberry composition associated with the large new group is summarized in Table 6; (4) that within the new group, SiO_2 content can vary from 0 wt% (which corresponds to no silicate minerals in blueberries at all) to somewhere around 8 wt% (which corresponds to the upper limit for consistency with the non-detection of silicates in blueberries) while (on average) the total content due to the five species MgO, Na_2O, P_2O_5, SO_3, and Cl remains stable at round 7 wt%; (5) that alterations to the group inclusion/rejection cut-off value for SiO_2 wt% do *not* change a defining feature of the composition distributions included in the large, new group, namely the total content due to the five species MgO, Na_2O, P_2O_5, SO_3, and Cl is well above trace levels and, on average, is around 7 wt%, so that this feature of the large, new group is robust to changes in the cut-off value for SiO_2 wt% with changes in the range of 0 wt% to 8 wt%.

However, the initial searches did not find many other complete solution sets. And many of these are easy to specify, given those already found. For example, the linear combination of the two example solutions ES1 and ES2 in Table 4, with mixing fractions of 0.75 for ES1 and 0.25 for ES1, will produce a new acceptable complete solution set with 1.12 wt% SiO2 and 91.21 wt% FeO in the set's blueberry distribution: This new solution set fits into the gap between the red scatter plot and the green scatter plot in Figure 4 for the B370 distribution. Indeed the whole gap between these red and green scatter plots can be filled with various linear combinations of pairs of complete solutions sets associated with the red and green scatter plots. And, of course, the same can be done for the other mixed-material distributions.

The initial searches found the largest group of complete solution sets by finding many examples in it. This is a good start. However, stronger search results are needed to find the holy grail of blueberry composition studies, that is, to find an accurate range of all possible blueberry compositions while minimizing this range to the greatest extent the data allows.

The quest for this holy grail will reach milestones if any of the following occur: (a) all groups of complete solution sets consistent with the non-detection of silicates are found; (b) it is demonstrated that all of these groups are found; (c) the full range or extent of any of these groups is mapped out; (d) reasonable geological/geochemical histories are described that lead to blueberry compositions consistent with the blueberry compositions associated with any of these groups; or, (e) it is rendered unlikely that any geological history could lead to the formation of blueberries with compositions consistent with the blueberry compositions associated with any group (and, hence, allow rejection of that group from further consideration). It is likely that the three groups already found are the only three. Demonstrating this soon is possible.

The APXS data on mixed-materials, basaltic soils, and dusty soils, as well as the homogeneity of the interiors of blueberries, the high quality composition data on Hawaiian blueberry analogs (Morris et al, 2005), the non-detection of silicates in blueberries (Calvin et al., 2009), and this analysis all point to blueberry compositions with hematite content of around 90 wt% or, perhaps, 99+ wt%. Top loose blueberries are very plentiful (Calvin et al., 2009) and can be harvested (picked from the tops of smooth sheet and plains ripple soil bedforms) (Olsen, 2021a) rather than mined (with blasting, drilling and digging). This means that top loose blueberries are an attractive source material for steel-making to produce sheet steel and steel powder to construct steel infrastructure for science on and around the Meridiani Planum.

Appendix : Additional details on the selection of the data investigated

The APXS data analyzed in this paper comes from *Opportunity*'s oxide abundance database stored in the file apxs_oxides_mer1.

This database file had records for 370 sample target composition distributions. Each record for a measured distribution included an identifier (ID), a classifying distribution type code, an unofficial name, the 16 measured oxide/element mass percentages for the distribution (although, for nickel, zinc and bromine these are given in derived mass percent in ppm), the 16 errors on these measurements, and notes on the normalization constant and measurement integration time.

type	Soil Undisturbed (SU)	Soil Disturbed (SD)	Soil Trench (ST)	Soil Crest (SC)	Rock Undisturbed (RU)	Rock Brushed (RB)	Rock Ratted (RR)	Rock Ratted (RR1,RR2, RRB)	Cobble (C)	(CU)
number	36	18	4	0	193	55	46	9	0	9

Table A1. Numbers of database distributions by sample type.

The numbers of distributions by type in the database are given in Table A1. Only the two "berry bowl" measurements of the 212 measured distributions for rocks and cobbles are of interest to blueberry demixing, since for the main "berry bowl" measurement several blueberries were in the APXS's field of view (which was not the case for the other measured rock and cobble distributions). The two "berry bowl" distributions are not considered in this paper, but they may be analyzed in a future paper. The 18 disturbed soil and 4 trench soil distributions are of no interest to blueberry demixing. Soil crest distributions are now classified as undisturbed soils. All of the APXS distributions used here for demixing are now classified as undisturbed soils (SU), which has 36 sample distributions.

The blocked matrix presented in Figure 1 was blocked purely on the pairwise distance numbers and "blind" to the informal name annotation and without looking at MI photographs of the sample targets.

The two distributions in the minor block separating the two major blocks, *i.e.* B1974 and B237B, were each outliers to the two main blocks. The relatively short pairwise distances between the blueberry-mixture-like distribution B1974 and the distributions in the lower main block may be due to very high levels of dust sampled on sol 1974, since there was a thick layer of dust over the blueberries imaged by the MI on sol 1974 (see, for example, 1M303431159EFFA5BXP2976M2M1.JPG, but not reproduced here). No MI images were taken on sol 237, however all MI images for sol 238 (for example, 1M149323195EFF35CRP2999M2M1.JPG) show a basaltic soil with a contact plate impression and this soil had unusually low levels of cohesion (it was sand-like) relative to other basaltic soils imaged.

878 The MI images (documenting sample-targets) associated with the 22 distributions in the
879 largest of the matrix blocks in Figure 1 all showed blueberries, blueberry fragments or both, and
880 most sols included images with contact plate impressions into the blueberry-containing mixtures.
881 The MI images for four of the sample distributions (*i.e.* B369, B420B, B420 and B1647) were
882 dominated by blueberry fragments in fragment ripples (indicated by a light-blue color in the
883 vertical color-bar in Figure 1). The three distributions for the last three rows of the largest block
884 in Figure 1 (*i.e.* B1145, B1148 and B023) all had relatively small numbers of blueberries in their
885 associated MI sample target images. In contrast, the MI sample target images for distribution
886 B1647 showed large numbers of large blueberry fragments. The Jensen-Shannon pairwise
887 distances between distribution B1647 and the other distributions in the main block were
888 relatively large. These large distances imply there is something noticeably different about the
889 sample target for B1647, perhaps the target contained some chunks of Burns Formation
890 sediment, the images of the sample target also showed thick layers of dust over the blueberry
891 fragments. The distributions B1145, B1148 and B023 were not chosen for demixing due to their
892 low blueberry content, while B1647 was not chosen because the sample mixture likely contained
893 material beyond blueberries, blueberry fragments, basaltic soil and dust. Of the largest block's 18
894 remaining distributions eight (*i.e.* B911, B091, B1140, B1755, B509, B100, B420, and B825)
895 were not chosen for demixing since these distributions were all very similar to other
896 distributions, and, hence, are considered alternate, redundant distributions. This leaves the
897 following 10 mixed-material distributions that are chosen for demixing: B369, B910, B080,
898 B420B, B505, B370, B2224, B443, B1136, and B416.

899 The 12 sample distributions in the second large block were ordered so that two major
900 sub-blocks are apparent. Cross referencing with the archive of MI images shows that the
901 distributions associated with the first sub-block (*i.e.* B3373, B730, B011, B249, B166, and
902 B3925) were measured from basaltic soil targets with large grain sizes and only a thin dust layer,

903 while the MI images associated with the second sub-block distributions (*i.e.* B3925, B3836,
904 B123, B060, B2957, and B3475) indicated that the sample targets had thick top-layers of light,
905 fine-grained dust. Although, *Opportunity*'s MI image archive associated with the relevant sols
906 for this block was quite sparse - no MI images were taken on sols 730 and 3630, none again on
907 sols 12 and 166 (although MI images of basaltic soils were taken on sols 12 and 167), no MI
908 images were taken on sol 60 (but this is the "MontBlanc_LesHauches" measurement that Morris
909 et al. (2006) emphasize as a dusty soil target) while no contact plate impressions are seen in the
910 MI images for sols 3925, 3836 and 2957. Five of the basaltic soil distributions (*i.e.*, B3373,
911 B011, B249, B166, and B3630) and four of the dusty distributions (*i.e.*, B3836, B123, B060, and
912 B3475) were chosen as filtering distributions in the demixing computations. The B730, B3925,
913 and B2925 distributions were omitted because of a combination of redundancy with other
914 distributions and a lack of MI photographic documentation of the sample targets. Although,
915 B3925 later proved useful for defining the layer thickness of the outer layer of the space of dusty
916 soil distributions.
917

918 **Acknowledgments**

919 The sole author had no funding from any source, and has no financial conflict of interest.

920 **Open Research**

921 The APXS data used for searching mass-balance analysis in the study are available at the PDS
922 Geosciences (GEO) Node and in the file apxs_oxides_mer1.Opportunity.csv via
923 doi:10.17189/1518973 or https://an.rsl.wustl.edu/merb/merxbrowser/an3.aspx and is in the Public
924 Domain (CCO).
925

926 The PanCam image data used for checking sampling locations are available at the PDS
927 Geosciences (GEO) Node and NASA's *Opportunity* raw image archive at doi:10.17189/1518971 and
928 https://mars.nasa.gov/mer/gallery/all/opportunity.html and is in the Public Domain (CCO).
929

930 The complete solution set data generated from the APXS data by the current research are available
931 at the Zenodo Generalist Repository (zenodo.org) via doi:10.5281/zenodo.5787305 with open
932 access (a Creative Commons, CCO, license)
933
934

References

Arvidson, R. E., Poulet, F., Morris, R.V., Bibring, J.P., Bell III, J.F., Squyres, S.W., et al. (2006). Nature and origin of the hematite-bearing plains of Terra Meridiani based on analyses of orbital and Mars Exploration rover data sets. *Journal of Geophysical Research: Planets*, 111, E12S08. https://doi.org/10.1029/2006JE002728

Bell, J. F., III, Squyres, S.W., Herkenhoff, K.E., Maki, J.N., Arneson, H.M., Brown, D., et al. (2003). Mars Exploration Rover Athena Panoramic Camera (PanCam) investigation. *Journal of Geophysical Research: Planets*, 108(E12), 8063. https://doi.org/10.1029/2003JE002070

Bell, J. F., III, Squyres, S.W., Arvidson, R.E., Arneson, H.M., Bass, D., Calvin, W., et al. (2004). PanCam multispectral imaging results from the Opportunity Rover at Meridiani Planum. *Science*, 306 (5702), 1703–1709. https://doi.org/10.1126/science.1105245

Braun, R., & Manning, R. M. (2007). Mars Exploration Entry, Descent, and Landing Challenges. *Journal of Spacecraft and Rockets*, 44(2), 310–328. https://doi.org/10.2514/1.25116

Calvin, W. M., Shoffner, J. D., Johnson, J. R., Knoll, A. H., Pocock, J. M., Squyres, S. W., et al. (2009). Hematite spherules at Meridiani: Results from MI, Mini-TES, and PanCam. *Journal of Geophysical Research: Planets*, 113, E12S37. https://doi.org/10.1029/2007JE003048.

Christensen, P. R., Bandfield, J.L., Clark, R.N., Edgett, K.S., Hamilton, V.E., Hoefen, T., et al. (2000). Detection of crystalline hematite mineralization on Mars by the Thermal Emission Spectrometer: Evidence for near-surface water. *Journal of Geophysical Research: Planets*, 105, 9623–9642. https://doi.org/10.1029/1999JE001093

Christensen, P. R., Mehall, G.L., Silverman, S.H., Anwar, S., Cannon, G., Gorelick, N., et al. (2003). Miniature Thermal Emission Spectrometer for the Mars Exploration Rovers. *Journal of Geophysical Research: Planets*, 108(E12), 8064. https://doi.org/10.1029/2003JE002117

Christensen, P. R., & Ruff, S. W. (2004). Formation of the hematite-bearing unit in Meridiani Planum: Evidence for deposition in standing water. *Journal of Geophysical Research: Planets*, E08003. https://doi.org/10.1029/2003JE002233

Christensen, P. R., Wyatt, M.B., Glotch, T.D., Rogers, A.D., Anwar, S., Arvidson, R.E., et al. (2004). Mineralogy at Meridiani Planum from the Mini-TES Experiment on the Opportunity Rover. *Science*, 306, (5702), 1733–1739. https://doi.org/10.1126/science.1104909

Christensen, P. R., Ruff, S.W., Fergason, R., Gorelick, N., Jakosky, B.M., Lane, M.D., et al. (2005). Mars Exploration Rover candidate landing sites as viewed by THEMIS. *Icarus*, 176(1), 12–43. https://doi.org/10.1016/j.icarus.2005.01.004

Dunham, E. T., Balta, J. B., Wadhwa, M., Sharp, T. G., & McSween, H. Y. (2019). Petrology and geochemistry of olivine-phyric shergottites LAR 12095 and LAR 12240: Implications for their petrogenetic history on Mars. *Meteoritics & Planetary Science*, 54(4), 811–835. https://doi.org/10.1111/maps.13262

Edgett, K. S. (1997). Nature and source of low-albedo surface material in the sandy aeolian environment of Sinus Meridiani, Mars. *Geology Society of America Abstract Programs*, 29, A214.

Edgett, K. S., & Parker, T. J. (1997). Water on early Mars: Possible sub-aqueous sedimentary deposits covering ancient cratered terrain in western Arabia and Sinus Meridiani. *Geophysical Research Letters*, 24, 2897–2900. https://doi.org/10.1029/97GL02840

Fenton, L. K., Michaels, T. I., & Chojnacki, M. (2015). Late Amazonian aeolian features, gradation, wind regimes, and Sediment State in the Vicinity of the Mars Exploration Rover Opportunity, Meridiani Planum, Mars. *Aeolian Research*, 16, 75–99. https://doi.org/10.1016/j.aeolia.2014.11.004

Gellert, R., Rieder, R., Brückner , J., Clark, B. C., Dreibus, G., Klingelhöfer, G., et al. (2006). Alpha Particle X-Ray Spectrometer (APXS): Results from Gusev crater and calibration report. *Journal of Geophysical Research: Planets*, 111, E02S05. https://doi.org/10.1029/2005JE002555

Gorevan, S., Myrick, T., Davis, K., Chau, J. J., Bartlett, P., Mukherjee, S., et al. (2003). Rock Abrasion Tool Mars Exploration Rover Mission. *Journal of Geophysical Research: Planets*, 108(E12), 8068. https://doi.org/10.1029/2003JE002061

Herkenhoff, K. E., Squyres, S. W., Bell, III, J.F., Maki, J. N., Arneson, H. M., Bertelsen, P., et al. (2003). Athena Microscopic Imager investigation. *Journal of Geophysical Research: Planets*, 108(E12), 8065. https://doi.org/10.1029/2003JE002076

Jolliff, B. L., & the Athena Science Team (2005). Composition of Meridiani hematite-rich spherules: A mass-balance mixing model approach. In *Lunar Planetary Science, XXXVI*, Abstract 2269.

Jolliff, B. L., Clark, B. C., Mittlefehldt, D. W., Gellert, R., & the Athena Science Team (2007). Compositions of Spherules and Rock Surfaces at Meridiani. In *Seventh International Conference on Mars*, abstract 3374, Jet Propul. Lab., Pasadena, Calif.

Jolliff, B. L., Gellert, R., & Mittlefehldt, D. W. (2007b). More on the possible composition of the Meridiani hematite-rich concretions. In *Lunar Planetary Science, XXXVIII*, Abstract 2279.

Klingelhöfer, G., Morris, R. V., Bernhardt, B., Rodionov, D., de Souza Jr, P. A., Squyres, S. W., et al. (2003). Athena MIMOS II Mössbauer spectrometer investigation. *Journal of Geophysical Research: Planets*, 108 (E12), 8067. https://doi.org/10.1029/2003JE002138

Klingelhöfer, G., Morris, R.V., Bernhardt, B., Schröder, C., Rodionov, D.S., de Souza Jr., P.A., et al. (2004). Jarosite and Hematite at Meridiani Planum from Opportunity's Mössbauer Spectrometer. *Science*, 306 (5702), 1740–1745. https://doi.org/10.1126/science.1104653

Mars Exploration Rover APXS Team. (2016). MER APXS Derived Oxide Data Bundle. PDS Geosciences (GEO) Node. https://doi.org/10.17189/1518973

Mars Exploration Rover Microscopic Imager Team (2016). MER1 Microscopic Imager Science Raw Data Bundle. PDS Geosciences (GEO) Node. https://doi.org/10.17189/1518971

Morris, R. V., Golden, D. C., Bell III, J. F., Shelfer, T. D., Scheinost, A. C., Hinman, N. W., et al. (2000). Mineralogy, composition, and alteration of Mars Pathfinder rocks and soils: Evidence from multispectral, elemental, and magnetic data on terrestrial analogue, SNC meteorite, and Pathfinder samples. *Journal of Geophysical Research: Planets*, 105, 1757–1817. https://doi.org/10.1029/1999JE001059

Morris, R.V., Ming, D. W., Graff, T. G., Arvidson, R. E., Bell III, J. F., Squyres, S. W., et al. (2005). Hematite spherules in basaltic tephra altered under aqueous, acid-sulfate conditions on Mauna Kea volcano, Hawaii: Possible clues for the occurrence of hematite-rich spherules in the Burns formation at Meridiani Planum, Mars. *Earth and Planetary Science Letters*, 240, 168–178. https://doi.org/10.1016/j.epsl.2005.09.044

Morris, R. V., Klingelhöfer, G., Schröder, C., Rodionov, D.S., Yen, A., Ming, D.W., et al. (2006). Mössbauer mineralogy of rock, soil, and dust at Meridiani Planum, Mars: Opportunity's journey across sulfate-rich outcrop, basaltic sand and dust, and hematite lag deposits. *Journal of Geophysical Research: Planets*, 111(E12S15), 8068. https://doi.org/10.1029/2006JE002791

Olsen, R. M. (2021a). Iron Oxide Harvesting on Mars. In *AIAA ASCEND 2021*, 4037, Las Vegas, Nevada & Virtual. https://doi.org/10.2514/6.2021-4037

Olsen, R. M. (2021b). Searching Mass-Balance Analysis to Find the Composition of Martian Blueberries: Database of Complete Solution Sets. Zenodo. https://doi.org/10.5281/zenodo.5787305

Pang, K-N, Li, C., Zhou, M-F., & Ripley, E.M. (2008). Abundant Fe–Ti oxide inclusions in olivine from the Panzhihua and Hongge layered intrusions, SW China: evidence for early saturation of Fe–Ti oxides in ferrobasaltic magma. *Contributions to Mineralogy and Petrology*, 158, 307-321. https://doi.org/10.1007/s00410-008-0287-z

Rieder, R., Gellert, R., Brückner, J., Klingelhöfer, G., Dreibus, G., Yen, A., & Squyres, S.W. (2003). The new Athena alpha particle X-ray spectrometer for the Mars Exploration Rovers. *Journal of Geophysical Research: Planets*, 108 (E12), 8066. https://doi.org/10.1029/2003JE002150

Rieder, R., Gellert, R., Anderson, R.C., Brückner, J., Clark, B.C., Dreibus, G., et al. (2004). Chemistry of Rocks and Soils at Meridiani Planum from the Alpha Particle X-ray Spectrometer. *Science*, 306 (5702), 1746–1749. https://doi.org/10.1126/science.1104358

Soderblom, L. A., Anderson, R.C., Arvidson, R.E., Bell III, J.F., Cabrol, N.A., Calvin, W., et al. (2004). Soils of Eagle Crater and Meridiani Planum at the Opportunity Rover Landing Site. *Science*, 306(5702), 1723–1726. https://doi.org/10.1126/science.1105127

Squyres, S. W., Arvidson, R. E., Baumgartner, E. T., Bell III, J. F, Christensen, P. R., Gorevan, S., et al. (2003). Athena Mars Rover science investigation. *Journal of Geophysical Research: Planets*, 108 (E12), 8062. https://doi.org/10.1029/2003JE002121

Squyres, S. W., Grotzinger, J.P., Arvidson, R.E., Bell III, J.F., Calvin, W., Christensen, P.R., et al. (2004). In Situ Evidence for an Ancient Aqueous Environment at Meridiani Planum, Mars. *Science*, 306 (5702), 1709–1714. https://doi.org/10.1126/science.1104559

Tirsch, D., Craddock, R.A., Platz, T., Maturilli, A., Helbert, J., & Jaumann, R. (2012). Spectral and petrologic analyses of basaltic sands in Ka'u Desert (Hawaii) – implications for the dark dunes on Mars. *Earth Surface Processes and Landforms*, 37, 434–448. https://doi.org/10.1002/esp.2266